PROCEEDINGS, Twenty-First Workshop on Geothermal Reservoir Engineering
Stanford University, Stanford, California, January 22-24, 1996
SGP-TR-151

INJECTION PLUME BEHAVIOR IN FRACTURED, VAPOR-DOMINATED RESERVOIRS

Karsten Pruess

Earth Sciences Division, Lawrence Berkeley National Laboratory
University of California, Berkeley, CA 94720

Abstract

We discuss fluid flow and heat transfer processes during water injection into hot, fluid-depleted vapor zones. Numerical simulations of injection plumes in fractures, modeled as two-dimensional heterogeneous porous media, indicate complex behavior. Under certain conditions it is possible to make detailed quantitative predictions of vaporization behavior. However, when effects of reservoir heterogeneity are dominant it will only be possible to predict the behavior of injection plumes in general terms.

Introduction

In response to extensive steam production, the vapor-dominated geothermal reservoirs at The Geysers, California, and Larderello, Italy, are beginning to run out of fluid, while heat reserves in place are still enormous. Injection of water is the primary means by which dwindling fluid reserves can be replenished, and recovery of thermal energy be enhanced and accelerated. Field experience shows that water injection may have very beneficial effects, increasing reservoir pressures and flow rates of offset steam production wells (Beall et al., 1989; Enedy et al., 1991; Goyal and Box, 1992; Goyal, 1995). Effects of water injection are not always favorable, however, because thermal degradation (temperature decline) or water breakthrough may occur at neighboring wells (Barker et al., 1992).

Large-scale permeability at The Geysers and Larderello is provided by networks of interconnected fractures (Beall and Box, 1989), while the matrix rock has low permeability typically of order 10^{-18} m^2 (1 microdarcy) or less. The ability of water injection to sustain steam production then depends on the rate of heat transfer from the reservoir rocks to water migrating along fractures. This paper is concerned with the fluid and heat flow processes that develop when liquid water enters hot sub-vertical fractures in rocks of low permeability. Fractures are modeled as two-dimensional heterogeneous porous media with rough walls, bounded by semi-infinite rock slabs. The descent of boiling liquid plumes in such fractures under the combined action of gravity, capillary, and pressure forces is analyzed by means of high-resolution numerical simulations, using our TOUGH2 general-purpose reservoir simulator (Pruess, 1991a), enhanced with a set of preconditioned conjugate gradient solvers (Moridis and Pruess, 1995). We also present a lumped model for plume migration and vaporization, using simple approximations for fluid flow in the fracture and for conductive heat transfer from the wall rocks.

General description of injection plume behavior.

Injection of water into hot sub-vertical fractures gives rise to a complex interplay of multiphase fluid flow and heat transfer processes. Two-phase flow in the plume takes place under the combined action of gravity, capillary, and pressure forces. Liquid water will also partially imbibe into the rock matrix. In open sections of fractures water will flow generally downward, driven by gravity. However, at asperity contacts (fracture walls touching) water may pond and be diverted sideways. In regions of small fracture apertures or strong wall roughness, capillary pressure effects could also be significant.

Conductive heat transfer from the wall rocks causes the temperature of the water to increase, and eventually boiling is initiated when the water reaches the saturation temperature at prevailing pressure, $T_{sat}(P_0)$. Thermal diffusivities of rocks are low, typically of the order of 10^{-6} m^2/s. Thus, heat conduction to the injection plume is a relatively slow process, giving rise to very broad two-phase zones (Calore et al., 1986). This is in contrast to liquid injection into hot underpressured porous media, where rock-fluid heat transfer occurs over small spatial scales (grain sizes), with rapid thermal equilibration locally and "sharp" two-phase fronts (Schroeder et al., 1982; Pruess et al., 1987).

The vaporization process is accompanied by an increase in pressure which drives the steam away from the injection plume. Two parameter regimes may be distinguished. When water enters a fracture at a "low" rate, the rates of vapor generation and flow are also small, causing an insignificant increase in pressure. Plume pressure P_{pl} remains close to initial fluid pressure P_0 and, because of the one-to-one

correspondence between pressures and temperatures in two-phase conditions, plume temperature $T_{pl} = T_{sat}(P_{pl}) \approx T_{sat}(P_0)$. Under "high-rate" conditions the rate of vapor flow is large, causing significant pressure gradients to develop, and plume pressures to rise substantially, $P_{pl} >> P_0$. Plume temperature $T_{sat}(P_{pl})$ will then also be considerably larger than $T_{sat}(P_0)$. Outside the region swept by the injection plume, single-phase vapor flow occurs under nearly isothermal conditions, at original reservoir temperature T_0.

The boiling injection plume is a very efficient heat transfer system, operating by means of vapor-liquid counterflow (heat pipe; Calore et al., 1986). In hotter regions, at larger distance from the injection point, vapor pressures are larger than in cooler portions of the plume. Accordingly, vapor will flow from the hotter to the cooler regions (generally towards the injection point, opposing liquid flow which is generally directed away from the injection point). The hotter regions are zones of evaporation, in which latent heat is consumed, while in the cooler regions condensation is taking place, accompanied by deposition of latent heat. The latent heat transfer coupled with vapor flow tends to equalize temperatures throughout the two-phase plume.

The strength of the gravitational body force acting on liquid water with density ρ_l is equivalent to a pressure gradient of $\rho_l g$, which for typical conditions of $T \approx 220$ °C is approximately 8 kPa/m. For injection into underpressured vapor zones at $P \approx 10$ bar, $T \approx 240$ °C, the fluid pressure in two-phase sections of the plume is limited to $P_{pl} \leq P_{sat}(240\ ^\circ C) = 3.34$ MPa. For a plume pressure of 2.5 MPa ($T_{sat} = 224$ °C), the pressure gradient towards an offset producer at 200 m distance with a bottomhole pressure of 1 MPa would be 7.5 kPa/m on average, which is roughly of the same magnitude as the gravitational force. This suggests that vapor pressure gradients may have a strong impact on liquid flow as well. Depending on local heterogeneity conditions, liquid water may migrate to offset production wells at elevations comparable to the injection point. Additional complications arise from hydrodynamic instabilities, including the gravitational instability of water over steam (Pruess, 1991b), and viscous instabilities at the water-vapor interface (Fitzgerald et al., 1994).

Injection plumes in heterogeneous fractures.

Fracture model

Rock fractures occur in a tremendous variety of sizes, from microcracks that are barely visible to the human eye all the way to large fractures extending over tens of meters or more. In the present work we are interested in fracture flow on a macroscopic scale (tens to hundreds of meters), for which a pore-level description of heterogeneity is not feasible. We use a macroscale continuum approach in which a fracture is represented as a two-dimensional heterogeneous porous medium, with appropriate small void space and large, pointwise-varying permeability (Pruess and Tsang, 1990). Stochastic permeability distributions are generated by computer to incorporate features that we believe to be essential characteristics of fractures in hard rocks of very low intrinsic permeability, such as the graywackes at The Geysers. Specifically, we assume that (1) permeability in the fracture plane varies with position in a gradual, spatially-correlated manner; (2) over some portions of the fracture surface the walls are in actual contact, i.e., in some regions fracture apertures are not only small but are actually zero. Note that, because of the postulated spatial correlation, fracture apertures will be very small near the asperities, and will gradually increase with distance from the asperity contacts.

Matrix permeability of the unfractured rocks at The Geysers and Larderello geothermal fields is typically of order 10^{-18} m^2 (1 microdarcy) or lower. This is very small in comparison to typical permeabilities of tens or hundreds of darcies (10^{-11} - 10^{-9} m^2) in the fracture plane. Thus, rock matrix permeability will have little impact on injection plume behavior over shorter time periods (days), although vapor adsorption and water imbibition into the rock matrix may be important long-term effects. This paper is concerned with flow of injected water in the fracture plane over relatively short time periods (days); accordingly, matrix permeability is neglected.

A synthetic heterogeneous permeability field that can represent a fracture is shown in Fig. 1. A two-dimensional square domain is discretized into 100x100 = 10,000 blocks, each of which is assigned a permeability $k_{ij} = \zeta_{ij} \times k_{ref}$. Here k_{ref} is a "reference" permeability, and the ζ_{ij} are "permeability multipliers," generated as a spatially-correlated stochastic field from a shifted log-normal distribution, using the turning bands method as implemented by Tompson (1989). Spatial correlation lengths are 1 in the horizontal direction, 0.5 in the vertical (in grid units). A fraction of 26.4 % of the area of the stochastic field shown in Fig. 1 has $\zeta_{ij} = 0$, corresponding to asperity contacts.

The 100x100 grid shown in Fig. 1 is subdivided into four grids of 50x50 = 2,500 blocks, and the four sets of permeability modifiers are assigned to finite-difference meshes of 50x50 blocks of 1 cm thickness and 10x10 m^2 area. This provides us with four 500x500 m^2 fractures that represent different realizations of the same heterogeneity structure (same

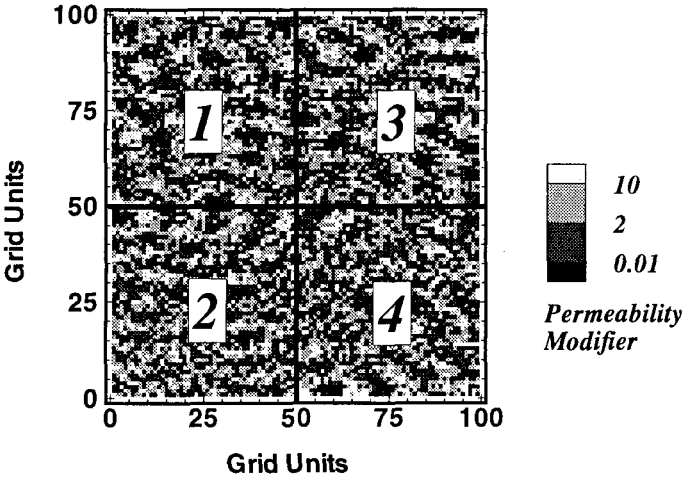

Figure 1. A spatially-correlated random field for representing heterogeneous fractures. Spatial correlation length is 1 grid unit in the horizontal direction, 0.5 units in the vertical. Permeability modifiers in the four quadrants labeled 1 - 4 are used separately in numerical simulation experiments.

mean, variance, and spatial correlation of permeability). Intrinsic porosity of the fractures is chosen as $\phi = 0.35$, corresponding to an open space with an average width of 3.5 mm between the fracture walls. The reference permeability of $k_{ref} = 10^{-9}$ m^2 is present over a region of 1 cm thickness, so that the reference permeability-thickness product of the fracture is 10^{-11} m^3, or 10 darcy-meters.

Semi-infinite slabs of matrix rock are attached to both fracture walls, to provide conductive heat transfer to the injection plume. While fluid and heat flow in the fracture plane is treated by numerical simulation, conductive heat transport in the matrix rock adjacent to the fracture is handled with the semi-analytical method of Vinsome and Westerveld (1980). This effectively reduces the three-dimensional fluid and heat flow problem to two dimensions. For heat conduction modeling it is assumed that the temperature at the fracture walls is identical to the temperature within the 1 cm thick fracture zone that is sandwiched between the walls. Initial conditions are a vapor-static equilibrium with an average pressure of P = 10 bars at a temperature of 240 °C. Relative permeability and capillary pressure curves are similar to those used by Pruess and Antunez (1995); effects of vapor adsorption and vapor pressure lowering are included. The capillary pressure functions are scaled consistently with permeability on a grid block-by-grid block basis according to $P_{cap} \rightarrow P_{cap'} = P_{cap}/\sqrt{(\zeta_{ij})}$ (Leverett, 1941). Water with an enthalpy of 100 kJ/kg, corresponding to a temperature of approximately 25 °C, is injected near the top, center of each of the four fractures at a rate of 10 kg/s. In all cases, the initial vapor-static pressure gradient is maintained at the right boundary of the fractures; all other boundaries are closed to heat and mass flow.

For comparison, we also simulated injection into a homogeneous fracture, with absolute horizontal and vertical permeabilities equal to the average permeabilities of the heterogeneous fractures. The overall average permeability of the (100x100 block) heterogeneous fracture was "measured" by numerical simulation, as follows. Two rows of grid blocks were attached to the top and bottom, respectively, of the heterogeneous fracture. Constant-pressure boundary conditions were then specified in these rows, and a single-phase isothermal flow simulation was run to steady state. Average vertical permeability was calculated from the steady flow rate and applied pressure drop, using Darcy's law. An analogous procedure was applied to obtain horizontal permeability, attaching two columns of grid blocks to the left and right edges of the heterogeneous fracture. The values $k_h = .69 \times k_{ref}$, $k_v = .36 \times k_{ref}$ obtained for the average horizontal and vertical permeabilities, respectively, were then used in the homogeneous fracture simulations.

Results

Injection plumes after 10^5 seconds (cumulative injection of 10^6 kg) in the heterogeneous fractures are shown in Fig. 2. For comparison, Fig. 3 shows the plume obtained for the homogeneous fracture. "Integrated" measures of plume behavior, including total liquid mass in the plume, and average plume temperature and liquid saturation, are shown in Figs. 4 - 6. The following observations can be made.

Apart from superficial differences in appearance, which are to be expected for different realizations of permeability fields with the same mean, variance, and spatial correlation lengths, the injection plumes in the four heterogeneous fractures have common features. Whereas the injection plume has a rather compact smooth shape in the homogeneous fracture, dendritic patterns with strong fingering are seen in the heterogeneous fractures. Generally speaking there is considerably stronger lateral flow in the heterogeneous fractures, and even some upward migration of injected water occurs locally. One may hope that homogeneous fracture models would be capable of capturing injection behavior in heterogeneous fractures "on average;" however, the heterogeneous fractures all show stronger lateral water migration than the homogeneous fracture, suggesting that the shape of the plume in the homogeneous fracture cannot be taken as representing an average of the heterogeneous plumes. It appears as though homogeneous reservoir models could seriously

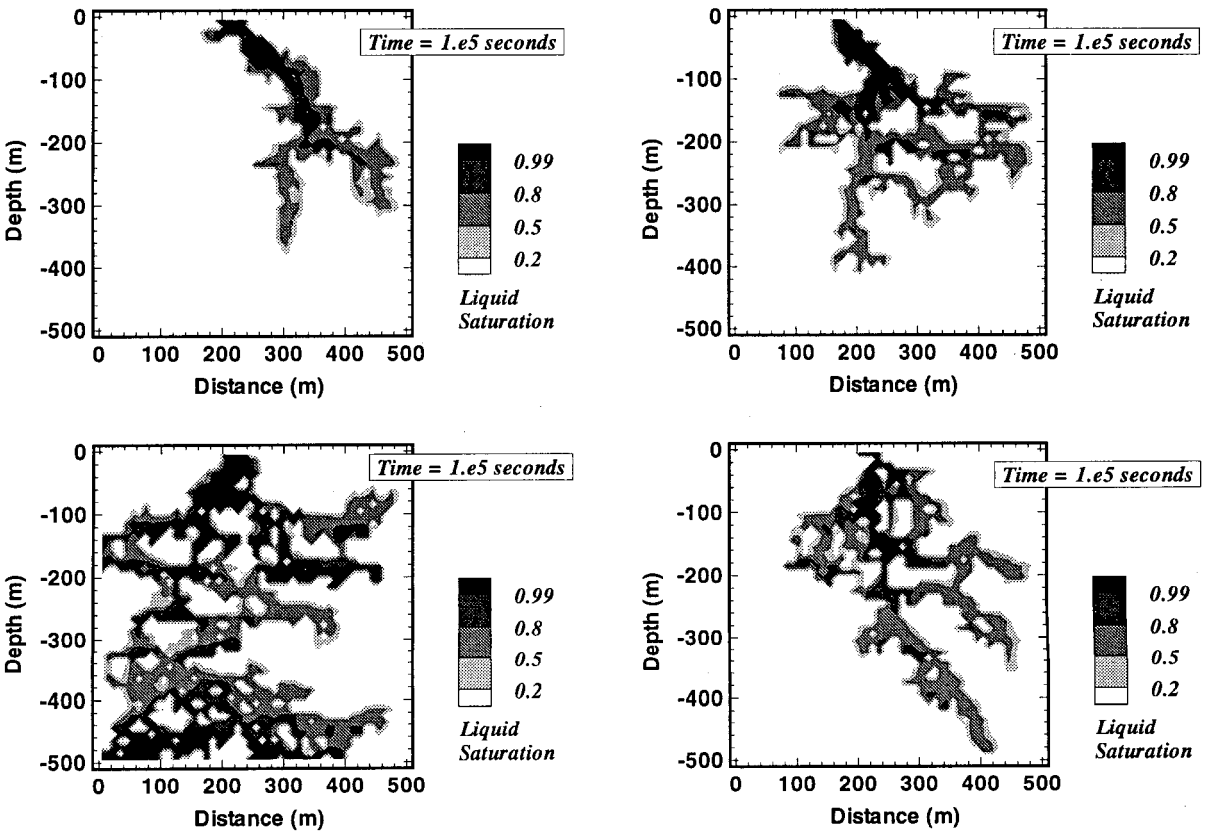

Figure 2. Simulated plumes for injection at a rate of 10 kg/s over 10^5 seconds into four heterogeneous fractures, corresponding to the four quadrants of the permeability field shown in Fig. 1.

underestimate the potential for breakthrough of liquid water at neighboring production wells.

The dendritic plume shapes obtained in heterogeneous fractures will provide more surface area for flow in the fracture plane, which would enhance vaporization. However, heterogeneous fractures may also have extended regions of small apertures, or even asperity contacts, which would tend to suppress flows and diminish vaporization. Fig. 4 shows that the four heterogeneous fractures have very different vaporization behavior. After injection of 10^6 kg of water, liquid mass present in the plumes ranges from (0.6 - 2.5) x 10^5 kg, indicating that, on average, 75 to 94 % of the injected fluid has been vaporized. Vaporization behavior in the homogeneous fracture is close to the average of the heterogeneous fractures at early times. Later, however, three of the four heterogeneous fractures show considerably stronger vaporization (less liquid mass in the plume) than is observed for the homogeneous case. Heterogeneous Fracture # 2 is an exception; it happens to include an extended region of low permeability, dipping at an angle of approximately 45°, which suppresses vapor flow from the boiling plume to the 10-bar pressure boundary at the right, hence diminishes vaporization.

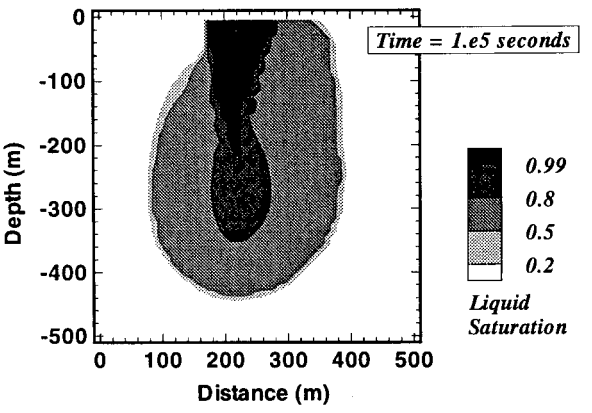

Figure 3. Simulated injection plume for a homogeneous fracture with permeability equal to the averages of the heterogeneous fractures.

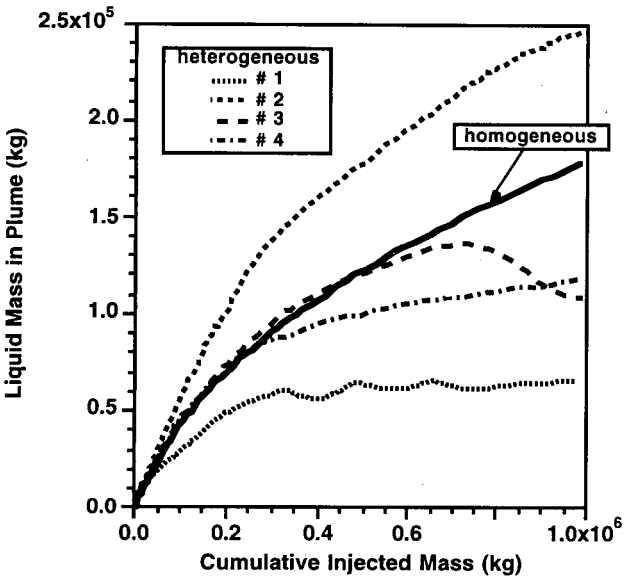

Figure 4. Growth of liquid mass in two-phase injection plumes with time for the four heterogeneous fractures and the homogeneous fracture.

A remarkable behavior is shown by Fracture # 3: liquid mass in the plume reaches a maximum at 7×10^4 seconds (7×10^5 kg injected), and subsequently actually declines even as injection is continuing (Fig. 4). Thus, in the period after 7×10^4 seconds, the rate of vaporization exceeds the rate of fluid injection! A more detailed analysis of plume behavior reveals that this surprising phenomenon is caused by an interplay between vapor pressures and liquid flows: in response to continuous vaporization fluid pressures in the fracture evolve, causing liquid flow patterns to change. Initially, liquid flow in Fracture # 3 is primarily downward, but there is also considerable lateral flow, some of which goes to the left, away from the constant pressure boundary. The liquid diverted to the left is vaporizing only slowly, because of flow resistance and pressure buildup over the long and circuitous flow path for the steam towards the right boundary. The lateral vapor pressure gradients eventually increase to a level where they divert a considerable fraction of liquid in the direction of the right $P \approx 10$ bar boundary, where vaporization occurs much more readily due to the shorter steam flow path.

Average plume temperatures (Fig. 5) show trends consistent with vaporization behavior and accumulation of liquid mass. Higher plume temperature generally corresponds with less vaporization, hence larger liquid mass. For the heterogeneous fractures, plume temperatures reach maximum values at early time and subsequently decline, although not necessarily in monotonic fashion. In contrast, for the homogeneous fracture plume temperature stabilizes after the early-time transient. Average liquid saturations in the plumes show very similar trends for three of the four heterogeneous fractures (Fig. 6). In the homogeneous fracture, average liquid saturation is considerably higher than in three of the four heterogeneous fractures. As was true for temperature, the liquid saturation of the homogeneous plume also stabilizes, after an initial transient, at a nearly constant value.

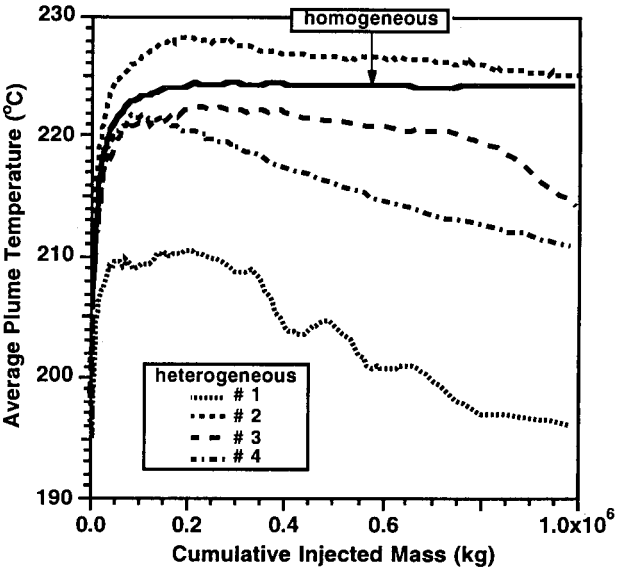

Figure 5. Average plume temperature as a function of injected mass.

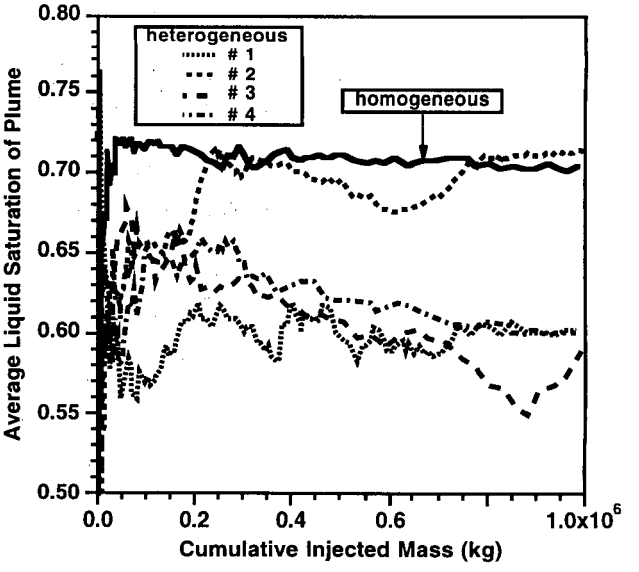

Figure 6. Average liquid saturation in injection plumes.

Low-rate injection into homogeneous fractures.

Water injection at high rates into heterogeneous fractures shows diverse and complex phenomena. In an effort to gain a better understanding of the interplay of fluid flow and heat transfer processes in injection plumes, we now focus on the simpler problem of low-rate injection into homogeneous fractures. The high-rate injection (10 kg/s) discussed previously would be relevant to flow in large fractures that directly intersect an injection well. Water flow at low rates may be expected in fractures at some distance from the injection well.

A series of numerical experiments was carried out in which water was injected at rates from 3.2 - 25.4 g/s into homogeneous anisotropic fractures of 20 m vertical and 14 m horizontal extent. Fracture permeabilities were taken to be the same as in the homogeneous case discussed above; initial conditions were again T = 240 °C, P ≈ 10 bars, and constant pressure conditions were maintained at the right boundary. A finite-difference grid with a resolution of $\Delta x = \Delta z = 0.2$ m was used.

Lumped-plume model

Before presenting simulation results for low-rate injection, we summarize a "lumped-plume model" (LPM), which attempts to describe overall average plume behavior in terms of a few spatially and temporally averaged parameters, using simple arguments of heat and mass conservation. For water injection at a rate q, total injected mass at time t is $M_{inj} = q\ t$. Of this, a fraction $f_{vap} = M_{vap}/M_{inj}$ is vaporized, while the remaining fraction $f_{liq} = 1 - f_{vap}$ is present as liquid in the boiling two-phase plume. By considering the "conductively-accessible" rock volume, we obtain the following relationship (Pruess, 1996)

$$\frac{q}{\left(f_{liq}\right)^2} = \alpha^2 M_{inj} + q \qquad (1),$$

where

$$\alpha = \frac{\sqrt{2\rho c K}\left(T_0 - T_{pl}\right)}{b \phi S_l \rho_l h_{vl}} \qquad (2).$$

α is a parameter group that depends on plume temperature and saturation, as well as on hydraulic parameters of the fracture, and thermal properties of the matrix rock. Parameters not previously defined are as follows: ρ, c, K are, respectively, density, specific heat, and thermal conductivity of the rock; b is width of the fracture, h_{vl} is heat of vaporization.

Results

At low injection rates, the increase of vapor pressure in the injection plumes is very small and, as expected, plume temperatures remain close to saturation temperature at initial pressure, $T_{pl} \approx T_{sat}(P_0)$. Plume temperature tends to increase with increasing injection rate, so that pressurization and associated lateral flow are also enhanced. Accordingly, plumes have vertically elongated finger-shapes at very low rates, while at increasing rates they broaden in the horizontal direction. For a given amount of injected water, liquid mass in the plume is larger (vaporization smaller) for larger injection rate, as the time available for supplying heat conductively to the fracture is smaller (Fig. 7). A remarkable result is

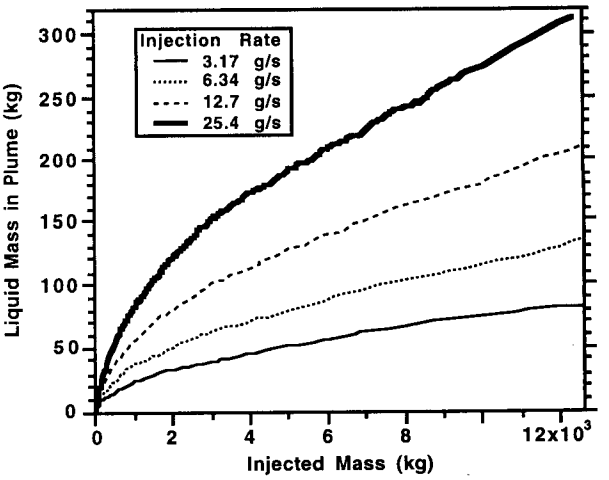

Figure 7. Growth of liquid mass in two-phase injection plumes with time for low injection rates.

that over time average liquid saturations in the plumes tend to stabilize (Fig. 8), with saturations larger for larger injection rates. With S_l independent of time, it then follows from Eqs. (1), (2) that the parameter group $q/(f_{liq})^2$ should plot as a straight line vs. injected mass. Fig. 9 shows that to a very good approximation this is indeed the case. In Table 1 we list the slopes α^2 read off Fig. 9 for the various injection rates, along with stabilized plume saturations S_l from Fig. 8. These parameters are used to calculate the parameter group $(\alpha S_l)^2$ which, according to Eq. (2), should be constant, regardless of injection rate; this is seen to be the case. Solving Eq. (2) for $(\alpha S_l)^2$ and inserting the parameters used in our simulations, the predicted value is $(\alpha S_l)^2 = .90 \times 10^{-3}$ s^{-1}, in excellent agreement with the values obtained in Table 1.

This analysis confirms the validity of our lumped plume model for the particular conditions investigated.

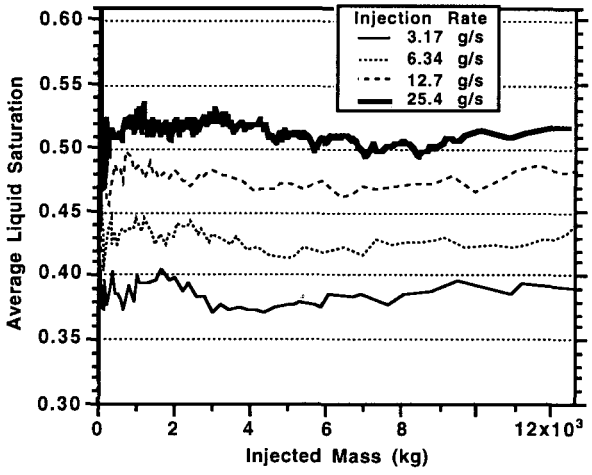

Figure 8. Average liquid saturations in injection plumes for low injection rates.

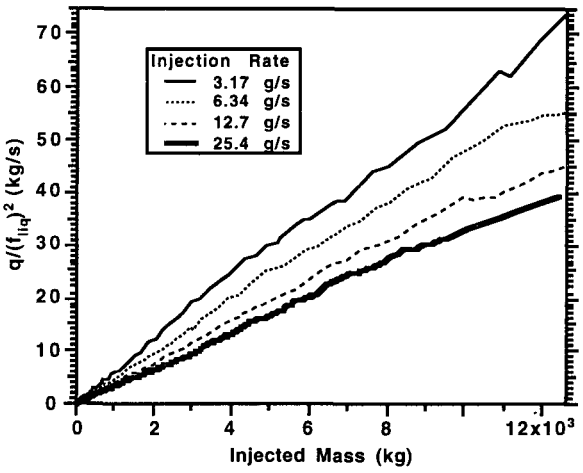

Figure 9. Parameter group from Eq. (1) versus injected mass.

q (g/s)	α^2 (s^{-1})	S_l	$(\alpha S_l)^2$ (s^{-1})
3.17	5.87e-3	.385	.87e-3
6.34	4.84e-3	.425	.87e-3
12.68	3.81e-3	.475	.86e-3
25.35	3.41e-3	.51	.89e-3

Table 1. Parameters for injection plumes.

Discussion and Conclusions.

Water injection into depleted vapor zones is an important tool for reservoir management at The Geysers and Larderello vapor-dominated fields. In this paper we have attempted to evaluate injection effects with due consideration to the heterogeneity of natural rough-walled rock fractures. Such fractures were modeled as two-dimensional heterogeneous porous media with stochastic spatially-correlated permeability structure in the fracture plane. This is believed to be more realistic than past approaches which conceptualized fractured media as homogeneous continua, although it still represents a considerable simplification relative to the irregular void space geometry of actual fractures and fracture networks (Beall and Box, 1989).

The behavior of injection plumes in heterogeneous fractures is very sensitive to the particular heterogeneity structure, which in actual applications will be highly site-specific and incompletely known at best. Nonetheless, injection plumes in heterogeneous fractures share common features. While injection into homogeneous media produces compact smooth-shaped plumes, heterogeneous fractures give rise to complex fingering flows with dendritic patterns. In heterogeneous fractures there is much stronger lateral flow, suggesting more potential for water interference at neighboring production wells than would be predicted from homogeneous fracture (or porous medium) models. This is in agreement with previous results in which a diffusion-analog was invoked to capture heterogeneity effects (Pruess, 1994). It appears that plume shapes in homogeneous fractures with the same average permeability do not represent an average of plume shapes in heterogeneous fractures.

Injection response is considerably simpler in homogeneous fractures for low water rates, such as may prevail at some distance from the injection well. The fraction of injected water remaining in liquid form (escaping vaporization) increases with injection rate. A remarkable observation from our simulations is that average water saturation in the plumes appears to stabilize at time-independent values, which are larger for larger injection rate. Our analysis of simulation results also suggests that average plume behavior may be described in terms of a lumped-parameter model.

Acknowledgement

The author is indebted to Drs. Curt Oldenburg and Marcelo Lippmann for their critical review of the manuscript and the suggestion of improvements. Thanks are due to Dr. Emilio Antunez for his help with the generation of spatially-correlated stochastic fields. This work was supported by the Assistant Secretary for Energy Efficiency and Renewable Energy, Geothermal Division, U.S. Department of Energy under Contract No. DE-AC03-76SF00098.

References

Barker, B.J., M.S. Gulati, M.A. Bryan, and K.L Riedel. Geysers Reservoir Performance, Special Report No. 17, Monograph on the Geysers Geothermal Field, pp. 167-177, C. Stone, (ed.), Geothermal Resources Council, Davis, CA, 1992.

Beall, J. J. and W. T. Box. The Nature of Steam Bearing Fractures in the South Geysers Reservoir, *Transactions, Geothermal Resources Council*, 13, 441-448, 1989.

Beall, J. J., S. Enedy and W. T. Box, Jr. Recovery of Injected Condensate as Steam in the South Geysers Field, *Geothermal Resources Council, Trans.*, 13, 351–358, 1989.

Calore, C., K. Pruess, and R. Celati. Modeling Studies of Cold Water Injection into Fluid-Depleted, Vapor-Dominated Geothermal Reservoirs, Proceedings, Eleventh Workshop Geothermal Reservoir Engineering, pp. 161-168, Stanford University, Stanford, California, January 1986.

Enedy, S., K. Enedy and J. Maney. Reservoir Response to Injection in the Southeast Geysers, Proceedings, Sixteenth Workshop on Geothermal Reservoir Engineering, Stanford University, Stanford, CA, January 1991.

Fitzgerald, S.D., A.W. Woods, and M. Shook. Viscous Fingers in Superheated Geothermal Systems, Proceedings, Nineteenth Workshop on Geothermal Reservoir Engineering, pp. 217-221, Stanford University, Stanford, CA, January 1994.

Goyal, K. Injection Recovery Factors in Various Areas of the Southeast Geysers, California, *Geothermics*, Vol. 24, No. 2, pp. 167-186, 1995.

Goyal, K. P. and W. T. Box. Injection Recovery Based on Production Data in Unit 13 and Unit 16 Areas of The Geysers Field, Proceedings, Seventeenth Workshop on Geothermal Reservoir Engineering, pp. 103-109, Stanford University, Stanford, CA, January 1992.

Leverett, M. C., Capillary Behavior in Porous Solids, *Trans. Soc. Pet. Eng. AIME*, 142, 152-169, 1941.

Moridis, G. and K. Pruess. Flow and Transport Simulations Using T2CG1, a Package of Conjugate Gradient Solvers for the TOUGH2 Family of Codes, Lawrence Berkeley Laboratory Report LBL-36235, Lawrence Berkeley Laboratory, Berkeley, CA, 1995.

Pruess, K. TOUGH2 - A General Purpose Numerical Simulator for Multiphase Fluid and Heat Flow, Report No. LBL-29400, Lawrence Berkeley Laboratory, Berkeley, CA, May 1991a.

Pruess, K. Grid Orientation and Capillary Pressure Effects in the Simulation of Water Injection into Depleted Vapor Zones, *Geothermics*, 20 (5/6), 257-277, 1991b.

Pruess, K. Liquid-Phase Dispersion During Injection into Vapor-Dominated Reservoirs, Lawrence Berkeley Laboratory Report LBL-35059, Proceedings, Nineteenth Workshop on Geothermal Reservoir Engineering, pp. 43-49, Stanford University, Stanford, CA, January 1994.

Pruess, K. On Vaporizing Water Flow in Hot Rock Fractures, manuscript in preparation, 1996.

Pruess, K. and E. Antunez. Applications of TOUGH2 to Infiltration of Liquids in Media with Strong Heterogeneity, in: K. Pruess (editor). Proceedings of the TOUGH Workshop '95, Lawrence Berkeley Laboratory Report LBL-37200, pp. 69-76, March 1995.

Pruess, K., C. Calore, R. Celati and Y. S. Wu. An Analytical Solution for Heat Transfer at a Boiling Front Moving Through a Porous Medium, *Int. J. of Heat and Mass Transfer*, 30 (12), 2595-2602, 1987.

Pruess, K., and Y. W. Tsang. On Two-Phase Relative Permeability and Capillary Pressure of Rough-Walled Rock Fractures, *Water Resour. Res.*, Vol. 26, No. 9, pp. 1915-1926, September 1990.

Schroeder, R. C., M. J. O'Sullivan, K. Pruess, R. Celati and C. Ruffilli. Reinjection Studies of Vapor-Dominated Systems, *Geothermics*, 11 (2), 93-120, 1982.

Tompson, A.F.B. Implementation of the Three-Dimensional Turning Bands Random Field Generator, *Water Resour. Res.*, Vol. 25, No. 10, pp. 2227 - 2243, 1989.

Vinsome, P. K. W. and J. Westerveld. A Simple Method for Predicting Cap and Base Rock Heat Losses in Thermal Reservoir Simulators, *J. Canadian Pet. Tech.*, 19 (3), 87–90, 1980.